

ZNF687 Mutations in Severe Paget Disease of Bone Associated with Giant Cell Tumor

Giuseppina Divisato,¹ Daniela Formicola,¹ Teresa Esposito,¹ Daniela Merlotti,² Laura Pazzaglia,³ Andrea Del Fattore,⁴ Ethel Siris,⁵ Philippe Orcel,⁶ Jacques P. Brown,⁷ Ranuccio Nuti,² Pasquale Strazzullo,⁸ Maria Serena Benassi,³ M. Leonor Cancela,⁹ Laetitia Michou,⁷ Domenico Rendina,^{8,10} Luigi Gennari,^{2,10} and Fernando Gianfrancesco^{1,10,*}

Paget disease of bone (PDB) is a skeletal disorder characterized by focal abnormalities of bone remodeling, which result in enlarged and deformed bones in one or more regions of the skeleton. In some cases, the pagetic tissue undergoes neoplastic transformation, resulting in osteosarcoma and, less frequently, in giant cell tumor of bone (GCT). We performed whole-exome sequencing in a large family with 14 PDB-affected members, four of whom developed GCT at multiple pagetic skeletal sites, and we identified the c.2810C>G (p.Pro937Arg) missense mutation in the zinc finger protein 687 gene (*ZNF687*). The mutation precisely co-segregated with the clinical phenotype in all affected family members. The sequencing of seven unrelated individuals with GCT associated with PDB (GCT/PDB) identified the same mutation in all individuals, unravelling a founder effect. *ZNF687* is highly expressed during osteoclastogenesis and osteoblastogenesis and is dramatically upregulated in the tumor tissue of individuals with GCT/PDB. Interestingly, our preliminary findings showed that *ZNF687*, indicated as a target gene of the NFκB transcription factor by ChIP-seq analysis, is also upregulated in the peripheral blood of PDB-affected individuals with (n = 5) or without (n = 6) mutations in *SQSTM1*, encouraging additional studies to investigate its potential role as a biomarker of PDB risk.

Introduction

Paget disease of bone (PDB [MIM: 602080]) is a common metabolic bone disorder characterized by focal areas of increased osteoclastic bone resorption coupled with a disorganized increase in osteoblastic bone formation.^{1–3} These abnormalities disrupt normal bone architecture and result in enlarged and deformed bones in one (monostotic form) or more (polyostotic form) regions of the skeleton. In less than 1% of cases, pagetic tissue might undergo neoplastic transformation, resulting in osteosarcoma and, less frequently, in giant cell tumor of bone (GCT); only 117 cases of GCT associated with PDB (GCT/PDB) are reported in the literature.^{4–7} These tumors arise in bones affected by PDB, and can appear as multifocal lesions. Despite the fact that familial clustering has been described in PDB-affected individuals with GCT, the underlying genetic alterations and the molecular basis of tumorigenesis in pagetic tissue remain to be defined.

Genetic factors are important in the pathogenesis of PDB, and in many affected families, inheritance has been described as autosomal dominant. Since 2002, mutations in *SQSTM1* (MIM: 601530) have been identified in up to 40% and 10% of individuals with familial and sporadic PDB, respectively.^{8,9} Genome-wide association studies have suggested additional predisposition loci in individ-

uals with PDB who are negative for *SQSTM1* mutations.^{10,11} Recently, we reported on a large family with 14 members affected by PDB, four of whom developed GCT at single or multiple pagetic skeletal sites.¹² We excluded the presence of mutations in *SQSTM1* or in other genes known to be associated with PDB-related syndromes (*TNFRSF11A* [MIM: 603499], *TNFRSF11B* [MIM: 602643], *VCP* [MIM: 601023], and identified multiple chromosomal regions, potentially housing the causative mutation.^{12,13} We now report the identification of a heterozygous missense mutation in *ZNF687* (MIM: 6010568) in all affected members of the family and in seven additional unrelated individuals with GCT/PDB. The same mutation (c.2810C>G) and one additional mutation (c.725G>T) in *ZNF687* (GenBank: NM_020832.2) were also detected in two families and in some severe PDB cases (with earlier onset and an increased number of affected skeletal sites) from two cohorts of pagetic individuals with different genetic backgrounds and previously analyzed for *SQSTM1* mutations.^{14,15}

Subjects and Methods

Subjects

The pedigrees of familial PDB-affected individuals with GCT and the clinical features of the affected family members are

¹Institute of Genetics and Biophysics “Adriano Buzzati-Traverso,” National Research Council of Italy, 80131 Naples, Italy; ²Department of Medicine, Surgery and Neurosciences, University of Siena, Siena 53100, Italy; ³Laboratory of Experimental Oncology, Rizzoli Orthopaedic Institute, Bologna 40136, Italy; ⁴Bambino Gesù Children’s Hospital, Regenerative Medicine Unit, Rome 00146, Italy; ⁵Department of Medicine, Columbia University Medical Centre, New York, NY 10032, USA; ⁶Pôle Appareil Locomoteur, Service de Rhumatologie B, Hôpital Lariboisière, Assistance Publique–Hôpitaux de Paris, Paris 75010, France; ⁷Division of Rheumatology, Department of Medicine, Université Laval, Québec, QC 42178, Canada; ⁸Department of Medicine and Surgery, Federico II University, Naples 80131, Italy; ⁹Department of Biomedical Sciences and Medicine and Centre of Marine Sciences, University of Algarve, Faro 8005-139, Portugal

¹⁰These authors contributed equally to this work

*Correspondence: fernando.gianfrancesco@igb.cnr.it

<http://dx.doi.org/10.1016/j.ajhg.2015.12.016>. ©2016 The Authors

This is an open access article under the CC BY-NC-ND license (<http://creativecommons.org/licenses/by-nc-nd/4.0/>).

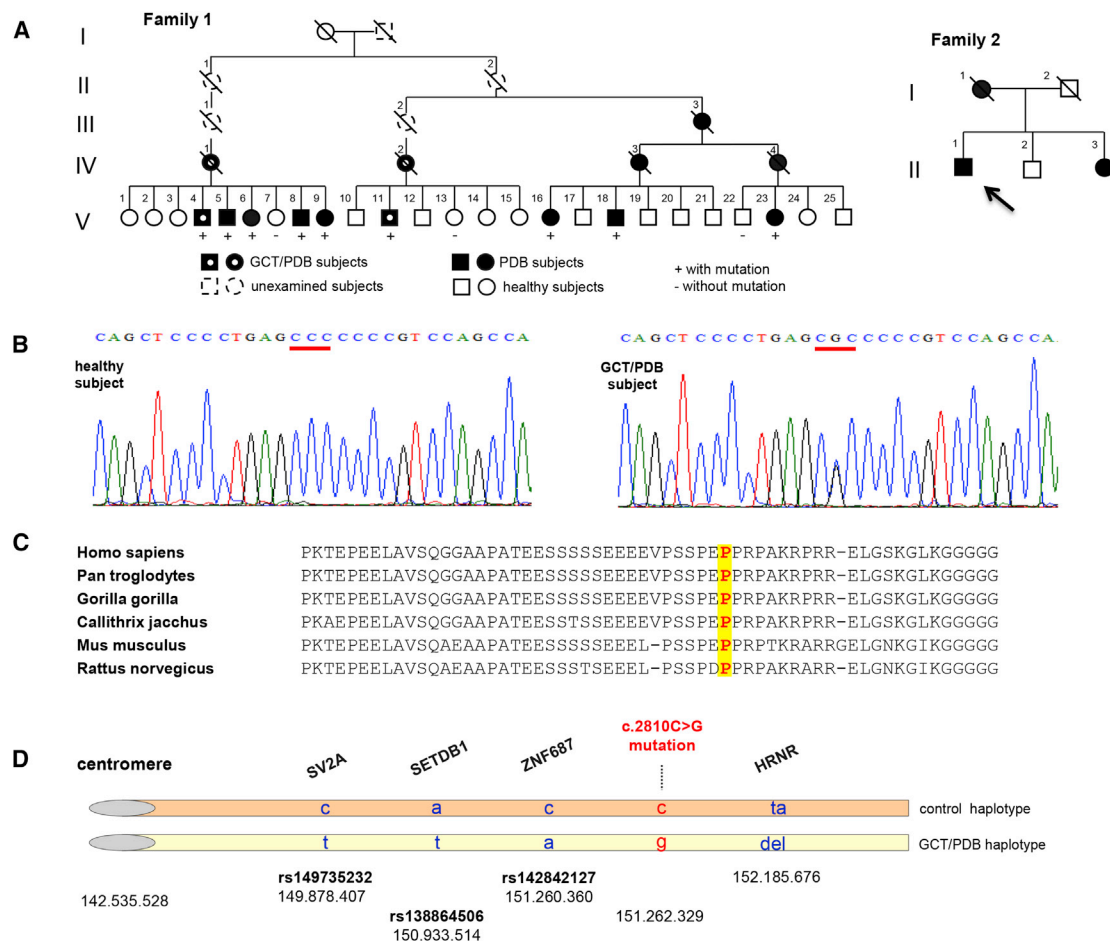


Figure 1. Identification of the c.2810C>G Mutation in *ZNF687*

(A) The pedigree of family 1, including 14 affected members, four of whom developed GCT at pagetic skeletal sites. Circles indicate female family members, and squares indicate male family members; slashes indicate that the family member is deceased. Family members with the GCT/PDB phenotype are indicated by a white dot in solid symbols, those with PDB are indicated by solid symbols, and those without any clinical symptoms are indicated by open symbols. + or - signs indicate the presence or absence of the c.2810C>G mutation. This panel also includes the pedigree for a different family (family 2) with the same c.2810C>G mutation in *ZNF687*. The index individual with PDB (II-1) is indicated by an arrow.

(B) The DNA sequence of a segment flanking c.2810C>G in *ZNF687* from an unaffected family member (left) and a heterozygous GCT/PDB-affected individual (right). A single base substitution changes the non-mutant cytosine to guanine, leading to the substitution of proline (P) for arginine (R) at the 937 codon (indicated by a solid line).

(C) A portion of the amino acid sequence of *ZNF687* from diverse mammal species.

(D) The ancestral haplotype with rare variants in *SV2A*-rs149735232 (t minor-allele frequency = 1.5%), *SETDB1*-rs138864506 (t minor-allele frequency = 0.1%), *ZNF687*-rs142842127 (a minor-allele frequency = 0.2%), and *HRNR* (ta deletion, frequency not available), all of which are genes surrounding the c.2810C>G mutation in *ZNF687*. For each variant, the position on chromosome 1 is indicated by arabic numerals.

provided in Figure 1A, Table 1, and Table S1. A replication cohort of seven unrelated PDB individuals with a history of GCT degeneration was also included in the study (Table 1). Moreover, 30 additional families affected by PDB, 20 of which were negative for mutation screening of *SQSTM1* or other genes associated with PDB-related syndromes, were also tested for *ZNF687* mutations. Then, we extended the screening of *ZNF687* mutations to two separate cohorts of PDB-affected individuals of Italian (n = 628) and multiethnic American (n = 342) backgrounds; these cohorts were previously analyzed for *SQSTM1* mutations. Unaffected control individuals of Italian (n = 564) and North-American (n = 269) origins were also screened as a reference. Clinical characteristics of PDB-affected individuals and control individuals are shown in the Supple-

mental Data (Table S2). The studies were approved by ethics review committees at the relevant institutions and all participants provided informed consent.

Whole-Exome Sequencing Strategy

Genomic DNA samples from four family members belonging to the extended pedigree were tested with the NimbleGen SeqCap EZ Exome™ capture kits (Roche), and the resultant fragments were sequenced on an Illumina GAIIX (Illumina) with 90 bp paired-end reads. Reads were obtained and aligned to the human reference genomic sequence (UCSC Genome Browser GRCh37/hg19) with MAQ7 and NextGENe software v.2.0. We adopted a prioritization scheme, described in Table S3, to identify the pathogenic mutation in each individual, similar to the approach

Table 1. Clinical Characteristics of Subjects with Familial and Sporadic PDB and Positive for *ZNF687* Mutations

Patient	<i>ZNF687</i> Mutation	Sex	Origin	GCT	PDB Onset (Age in Years)	No. of PDB sites	CHD
Family 1							
1.V-4	c.2810C>G	M	Italian	yes	35	12	yes
1.V-18	c.2810C>G	M	Italian	no	41	5	yes
1.V-11	c.2810C>G	M	Italian	yes	41	6	yes
Family 2							
2.II-1	c.2810C>G	M	Italian	no	45	4	yes
2.II-3	c.2810C>G	F	Italian	no	26	10	no
Family 3							
3.II-1	c.725G>T	M	Italian	no	50	4	yes
3.II-2	c.725G>T	F	Italian	no	59	2	yes
3.II-3	c.725G>T	F	Italian	no	43	3	yes
Unrelated Individuals with GCT/PDB							
GCT/PDB1	c.2810C>G	M	Italian	yes	33	7	yes
GCT/PDB2	c.2810C>G	F	Italian-American	yes	NA	2	NA
GCT/PDB3 ^a	c.2810C>G	F	Italian-American	no	NA	2	NA
GCT/PDB4 ^b	c.2810C>G	F	Italian-American	yes	NA	8	NA
GCT/PDB5	c.2810C>G	M	Italian	yes	38	7	yes
GCT/PDB6	c.2810C>G	M	Italian	yes	53	5	NA
GCT/PDB7	c.2810C>G	M	Italian	yes	46	5	NA
Unrelated Individuals with PDB							
PDB1	c.2810C>G	M	Italian	no	37	5	yes
PDB2	c.2810C>G	M	Italian	no	39	10	yes
PDB3	c.2810C>G	F	Italian	no	53	7	yes
PDB4	c.2810C>G	F	French-Canadian	no	61	2	NA
PDB5	c.2810C>G	F	French-Canadian	no	59	1	NA

M, male; F, female; PDB, Paget disease of bone; GCT, giant cell tumor of bone; CHD, coronary heart disease; NA, data not available.

^aMother and three siblings had PDB, mother also had GCT.

^bMother with PDB had either GCT or osteosarcoma.

used in our recent study.¹⁶ First, in order to reduce the number of candidate variants, we excluded the variants registered in the dbSNP131 and in our four in-house exomes, derived from four individuals with unrelated diseases and whose genetic basis was identified in our previous studies.^{16,17} After filtering, we compared data from three affected individuals (V-4, V-18, and V-11) to obtain shared variants, and we excluded those present in the healthy subject (V-7), thus identifying 57 variations in 45 genes (Table S4). Sanger sequencing allowed us to validate 21 out of these 57 variations.

Mutation Analysis of *ZNF687*

We conducted mutation screening of all 9 exons of *ZNF687* and their intron-exon boundaries by using PCR followed by automated DNA sequencing. PCR reactions (25 μ L) were performed with Taq

DNA polymerase (1 U; Fermentas), 1 \times buffer, deoxynucleoside triphosphate (dNTP, 0.2 mM; Amersham), primers (0.5 μ M), and DNA (100 ng). PCR conditions were as follows: initial denaturation at 94°C for 3 min, followed by 35 cycles of 94°C for 30 s, 30 s at annealing temperature, extension at 72°C for 45 s, and a final extension for 10 min at 72°C.

Samples were ExoSap-digested (Amersham) and sequenced with the Big Dye Terminator Ready Reaction Kit (Applied Biosystems). Sequencing reactions were performed with a 9700 Thermal Cycler (Applied Biosystems) for 25 cycles of 95°C for 10 s, 50°C for 5 s, and 60°C for 2 min. After sequencing, each reaction was column purified (Amersham) to remove excess dye terminators.

The sequencing of the products was performed with the ABI Prism 3710 Genetic Analyzer (Applied Biosystems).

Primers used for *ZNF687* amplification and sequencing are reported in [Table S5](#).

***ZNF687* Tissue Expression Pattern**

The tissue expression pattern of *ZNF687* was determined by real-time PCR ([Figure S3](#)) with the Light-Cycler system DNA Engine Opticon 2 (Biorad) and was performed on total RNAs derived from human adult tissues that were purchased from Stratagene. Total RNA was reverse transcribed with a RevertAid RT kit (Thermo Scientific). qPCRs were performed with SYBR Select Master Mix for CFX (Applied Biosystems) on a Bio-Rad CFX Connect Real-Time System instrument. The *ZNF687* transcript primers used to evaluate *ZNF687* mRNA expression are reported in [Table S5](#). *HPRT* primers were used to normalize *ZNF687* expression ([Table S5](#)). This experiment was carried out in triplicate.

Generation of Human Osteoclasts from PBMCs

Osteoclasts were generated in vitro, with peripheral blood mononuclear cells (PBMCs) from healthy volunteers and age- and sex-matched paigent individuals. PBMCs were isolated from citrate blood samples by density-gradient centrifugation in Ficoll (Histopaque 1077 Human Lymphocyte, Sigma-Aldrich), washed in 1× PBS, and re-suspended in alpha-minimal essential medium (α -MEM) (Sigma-Aldrich, Life Science), containing 100 U/mL penicillin, 100 mg/mL streptomycin (Gibco), 2 mM L-glutamine (Life Technologies) and 10% heat-inactivated fetal bovine serum (FBS). PBMCs were cultured in 96-well plates (8×10^5 cells per well) for RNA extraction, tartrate resistant acid phosphatase (TRAP) staining, and immunofluorescence. The cells were cultured in a humid atmosphere with 5% CO₂ in α -MEM and, after overnight incubation, the cultures were supplemented with 20 ng/mL of macrophage colony-stimulating factor (M-CSF; PeproTech) and 30 ng/mL of soluble human recombinant RANK ligand (sRANKL; PeproTech) and cultured for 14 days. Total RNA extraction was performed with TRIzol Reagent (Sigma-Aldrich), according to the manufacturer's protocol. Total RNA reverse transcription and qPCR were performed as described above. *ZNF687* expression profile during in vitro human osteoclastogenesis was obtained with the primers reported in [Table S5](#).

At the end of the culture, cells were fixed for 20 min at room temperature with 4% paraformaldehyde (Sigma-Aldrich) and stained for TRAP activity with a 87A Sigma Acid Phosphatase, Leukocyte (TRAP) Kit (Sigma-Aldrich). The nuclei were counterstained with methyl green. Multinucleated TRAP-positive cells were considered to be differentiated osteoclasts and were counted under a Zeiss microscope. For immunofluorescence assay, the TRAP+ cells were washed several times in 1× PBS and then incubated with 0.1% Triton X-100 (EuroClone) for 10 min at 4°C. Then, the cells were washed several times with 1× PBS and incubated with Texas RedX-phalloidin (Life Technologies) for 20 min. The nuclei were counterstained with DAPI. Slides were analyzed with a Zeiss Axioplan.

Generation of Human Osteoblasts from Molar Follicles

Normal human third-molar follicles were collected from tooth buds of healthy pediatric individuals, aged 8–12 years and who underwent extractions for orthodontics reasons, after obtaining informed consent from the parents of each individual. Dental follicles (DFs) were digested for 1 hr at 37°C in agitation in a solution of 3 mg/mL type I collagenase plus 4 mg/mL dispase (Gibco).

Single-cell suspensions were obtained by passing the cells through a 70 μ m BD Falcon strainer (Becton Dickinson). After filtration, single cell suspensions were seeded in a 25 cm² culture flask and cultured in α -MEM supplemented with 5% FBS, 100 U/mL penicillin-G, 100 μ g/mL streptomycin, and 0.25 μ g/mL fungizone (Gibco). Flasks were incubated at 37°C and 5% CO₂. For the induction of osteoblastic differentiation, the cells were grown in α -MEM supplemented with 2% FBS, 10⁻⁸ M dexamethasone, and 50 μ g/mL ascorbic acid (Sigma-Aldrich). For in vitro mineralized nodule evaluation, we cultured them for 30 days in α -MEM, supplemented with 10 mM β -glycerophosphate (Sigma-Aldrich). Total RNA extraction was performed with TRIzol Reagent (Sigma-Aldrich), according to the manufacturer's protocol. One μ g of total RNA was reverse transcribed as previously described. qPCRs were performed as previously described. *ZNF687* expression profile during in vitro human osteoblastogenesis was obtained with the primers reported in [Table S5](#).

Ethics Statement

Animal handling and experiments were legally accredited by the Portuguese Direcção Geral de Veterinária, and all the experimental procedures involving animals were performed according to the EU (Directive 86/609/CEE) and National (Portaria n° 1005/92 de 23 de Outubro; Portaria n° 466/95 de 17 de Maio; Portaria n° 1131/97 de 7 de Novembro) legislation for animal experimentation and welfare.

Fish Maintenance

Zebrafish eggs were obtained from natural spawning of in-house broodstock maintained in a ZebTec housing system (Tecniplast). Water parameters were maintained as follows: pH 7.6 \pm 0.2, conductivity 700 mS, dissolved oxygen 7.8 mg/L, and photoperiod 14:10 hr light:dark. Fertilized eggs were maintained until hatching in 1 L water tanks at a density of 200 eggs/L and with 0.5 ppm of methylene blue to avoid fungi development. Hatched larvae were raised until 30 days post-fertilization (dpf) in 1 L water tanks at a density of 100 larvae/L, and 90% of the water was renewed every 2 days. Larvae from 5 to 10 dpf were fed twice a day with *Artemia* nauplii (AF strain INVE, 5–10 nauplii/mL) and from 8 to 30 dpf with *Artemia* metanauplii (EG strain INVE, 10 metanauplii/mL). Juveniles, adults, and broodstock were maintained in 10 L plastic tanks with recirculating fresh water at 28°C (Tecniplast ZebTEC) and fed twice a day with commercial dry food (Tetramin flake C) and once a day with *Artemia* metanauplii.

Larval and Tissue Sampling

Fish embryos and larvae were sampled at 1 (4 cells), 3 (1,000–2,000 cells), 16 (14 somites), 24, 32, 48, 72, and 96 hr post-fertilization (hpf), and 5, 7, 9, 15, 20, and 30 dpf. The amount of material sampled at each developmental stage was adapted to specimen size and included about 100 eggs for the earliest developmental stages and five *Danio rerio* specimens for early juveniles (30 dpf). Adult zebrafish tissues (eye, operculum, vertebra, gills, liver, kidney, spleen, ovary, and scales) were collected and pooled from three males and two females. All fish were anesthetized with a lethal dose of tricaine methanesulfonate (MS-222; Sigma-Aldrich) and washed with sterile distilled water before sampling. For fin and blastema recovery, 20 adult fish were anesthetized, as mentioned above, and washed with PBS. Fins were then amputated, washed in PBS, and pooled to obtain

two biological replicates. 36 hr post-amputation (hpa), fish were re-anesthetized and the blastemas were recovered, washed with PBS, and pooled to obtain two biological replicates.

Specimens and tissues collected for gene-expression analysis were placed in ten volumes of TRI Reagent (Ambion) and stored at -80°C until processed.

Danio rerio RNA Extraction and qPCR

Total RNA was extracted from samples stored in TRI-Reagent, according to the manufacturer's instructions, and purified with a High Pure RNA Isolation Kit (Roche). RNA integrity was confirmed with an Experion Automated Electrophoresis System (Bio-Rad). Total RNA was reverse transcribed with M-MLV reverse transcriptase (Invitrogen), according to the manufacturer's protocol. qPCR was performed in triplicate with isoform-specific primers (Table S5). Levels of gene expression were calculated with the $\Delta\Delta\text{Ct}$ comparative method and normalized with housekeeping *rps18* (Table S5).

Bioinformatic Predictions

The NLStradamus program was used to predict the nuclear localization site of ZNF687.^{18,19} The NetPhos 2.0 server was used to predict serine, threonine, and tyrosine phosphorylation sites in ZNF687.²⁰

Immortalization and Cell Culture of Lymphoblasts

10 mL of blood were drawn from a peripheral vein, and lymphoblasts were isolated on a Ficoll-Diatrizoate density gradient (Ficoll-Paque; Pharmacia). B-lymphoblasts were immortalized by incubation with supernatant containing Epstein-Barr virus. After immortalization, B-lymphoblasts were grown for 10–14 days in RPMI 1640 medium (Gibco), supplemented with 2 mM L-glutamine, 100 U/mL penicillin, 100 mg/mL streptomycin (Gibco), and 20% FBS.

Cytoplasmic and Nuclear Protein Extraction from Lymphoblasts

The cells were washed with cold PBS (2.7 mM KCl, 1.2 mM KH_2PO_4 , 8.1 mM Na_2HPO_4 , 138 mM NaCl [pH 7.4]) and cytoplasmic extraction was obtained in 100–1,000 μL of hypotonic buffer (10 mM Tris-HCl [pH 7.5], 2mM MgCl_2 , 10 mM CaCl_2 , 30 mM Sucrose, 1% NP40) and $1\times$ proteinase inhibitor mixture (20 μg of 4-amidinophenyl-methanesulfonyl fluoride, 25 μg of antipain, 20 μg of aprotinin, 5 μg of nitobestatin, 20 μg of chymostatin, 25 μg of 3,4-dichloroisocoumarin, 50 μg of E-64, 10 μg of leupeptin, 10 μg of pepstatin A and 10 μg of phosphoramidon per mL, 50 μM bezamidine, 50 μM sodium metabisulfite). The lysis was performed with a syringe with a narrow-gauge (no. 27) hypodermic needle and was observed by the addition of a Trypan Blue solution. Then, the disrupted cells were centrifuged for 20 min at 10,000–11,000 rcf (relative centrifugal force). Nuclear extracts were sequentially obtained in 140 μL of extraction buffer (0.42 M NaCl, 0.2 mM EDTA, 25% Glycerol, 1% NP40) and $1\times$ proteinase inhibitor mixture. Crude nuclei were shaken gently and then incubated for 10 min on ice. Finally, nuclear extracts were obtained through centrifugation for 5 min at 20,000–21,000 rcf.

Western Blot Analysis for ZNF687 Cytoplasmic and Nuclear Localization

Proteins were denatured by being boiled in sample buffer, separated on 8% SDS-PAGE, transferred onto a Immun-Blot PVDF

Membrane For Protein Blotting (Bio-Rad), and blocked for 1 hr in 5% non-fat powdered milk in TBS-T (10 mM Tris-HCl [pH 7.5], 100 mM, NaCl, 0.1% [v/v] Tween-20). Rabbit polyclonal anti-ZNF687 antibody ab105544 (1:500 diluted in TBS-T; Abcam), α Tubulin (B-7) sc-5286 (1:500 diluted in TBS-T; Santa Cruz), and anti-RNA polymerase II ab815 (1:1,000 diluted in TBS-T; Abcam,) were used for protein detection. Peroxidase-conjugated goat anti-rabbit (1:1,000 for ZNF687) and anti-mouse (1:1,000 diluted in TBS-T for α tubulin and 1:2,000 diluted in TBS-T for RNA polymerase II; Bio-Rad) were used as secondary antibodies. Western blot assays were quantified with the ImageJ program.

RNA Extraction from Peripheral Blood of Pagetic Individuals

Venous blood derived from healthy volunteers and pagetic individuals (age- and sex-matched) was collected in a Tempus Blood RNA tube (Applied Biosystems) and immediately incubated at room temperature for 24 hr. RNA was extracted with a Tempus Spin RNA Isolation Reagent Kit (Applied Biosystems), and its quality was determined by a NANOD 1000 v.3.7.1 spectrophotometer (Thermo Scientific). Total RNA was reverse transcribed with RevertAid RT kit (Thermo Scientific) and qPCR was performed with the primers reported in Table S5. The experiment was carried out in triplicate.

GCT Tumor Tissues

The GCT/PDB tissue samples were obtained from surgically removed tumors, frozen in liquid nitrogen, and stored at -80°C . Total RNA was extracted from five frozen tumor tissues with TRIzol Reagent (Sigma-Aldrich), according to the manufacturer's protocol. Total RNA was reverse transcribed as previously mentioned, and qPCRs were performed in triplicate with the primers reported in Table S5.

Immunohistochemistry Assay

ZNF687 immunohistochemical analysis was performed on GCT paraffin-embedded microsections. H&E-stained slides were carefully reviewed, and the diagnosis of GCT/PDB was confirmed. Several sections of GCT/PDB tissue served as control tissue. A Dako LSAB 2 System HRP Kit (Universal Dako Labeled Streptavidin Biotin 2 System Horseradish Peroxidase) was used on formalin-fixed, paraffin-embedded material from primary tumors. Sections (5 μm thick) were deparaffinized in xylene and rehydrated in graded alcohols and water and the endogenous peroxidase was blocked by treating the sections with 0.3% H_2O_2 for 5 min at room temperature. Microwave pre-treatment was used to reveal the antigens to reduce nonspecific binding. The sections were incubated with blocking serum for 15 min, then at 4°C overnight with goat polyclonal anti-ZNF687 antibody (E-20 sc-324734; Santa Cruz) at the dilution 1:100. The sections were then incubated with the biotinylated secondary antibody and subsequently with ABC (avidin-biotin-peroxidase complex; Biomedica). The staining was developed in DAB (3,3'-Diaminobenzidine), and the nuclei were counterstained with hematoxylin. Positive controls were included for each antibody and negative controls were prepared without the incubation with the primary antibody. The staining was scored for intensity (0 = no expression, 1 = weak to moderate expression, 2 = strong expression) by two different investigators and for the percentage of positive cells (0 \leq 10%, 1 = 10%–25%, 2 = 26%–50%, 3 \geq 50%). Cut-off levels for the sum of scores were applied as for negative cases: 1–3 for weakly positive and 4–5 for

moderately to strongly positive, which is considered protein overproduction.

Results

Identification of *ZNF687* Mutations in GCT/PDB

The pedigrees of familial PDB individuals with GCT and the clinical features of the affected family members are provided in [Figure 1A](#), [Table 1](#), and [Table S1](#). Considering the high number of meiotic events in this extended pedigree, which reduces the number of candidate variants, we performed whole-exome sequencing of three affected PDB individuals (V-4, V-18, and V-11), two of whom had recurrent GCT, and one healthy subject (V-7) from family 1. We adopted a prioritization scheme, described in [Table S3](#), to identify the pathogenic mutation in each individual, similar to the approach used in our recent study.¹⁶ After excluding common SNPs and variants registered in the dbSNP131 and in our four in-house exomes (which are derived from four individuals with other diseases not related to bone metabolism, such as focal segmental glomerulosclerosis [MIM: 603278] and congenital fiber type disproportion [MIM: 255310]), we identified 21 candidate variants ([Tables S3](#) and [S4](#)). Only one showed precise cosegregation with the disease phenotype in the family: the c.2810C>G heterozygous change in exon six of *ZNF687*, which causes the p.Pro937Arg amino acid change ([Figure 1B](#)). *ZNF687* is localized on chromosome 1 (1q21.3), in one of the linkage candidate regions described in our previous report ([Figure S1](#)).¹²

Although its function has been poorly investigated, it is known that *ZNF687*, together with *ZMYND8* and *ZNF592*, is part of the recently described transcriptional regulator complex Z3.²¹

The proline residue at the 937 position of *ZNF687* is highly conserved in mammals ([Figure 1C](#)). The c.2810C>G mutation was not identified in a cohort of 564 unrelated healthy control individuals from the same geographical origin. Sanger sequencing confirmed the presence of the same c.2810C>G mutation (founder mutation) in all affected members of family 1, but not in unaffected members. Moreover, the same mutation was detected in seven additional unrelated individuals with PDB complicated with GCT ([Figure S4](#)). Four of these individuals were from the same circumscribed area of Southern Italy as family 1, and three were North-American individuals of European descent.^{14,15,22} In order to verify the hypothesis of a common ancestral chromosome among these GCT/PDB cases, we analyzed the segregation of rare variants in genes surrounding the *ZNF687* mutation, identifying, in all but one, identical variants for *SV2A* (MIM: 185860), *SETDB1* (MIM: 604396), *ZNF687*, and *HRNR* (MIM: 616293). This haplotype was not observed in any of the 564 control individuals of the same ethnic origin, suggesting that the c.2810C>G mutation originated from a unique haplotype and segregated in all but one of the GCT/PDB-affected individuals tested in this study ([Figure 1D](#)). The occurrence

of the c.2810C>G mutation on a different haplotype in one individual (individual GCT/PDB6) provides the genetic evidence that this mutation is necessary and sufficient for GCT/PDB phenotype development.

Identification of *ZNF687* Mutations in Individuals with Severe PDB

To determine the role of *ZNF687* in PDB-affected individuals without neoplastic transformation, we first analyzed the entire coding region of the gene in 30 additional PDB probands, 20 of whom were negative for *SQSTM1* mutations, as well as for mutations in other genes associated with PDB-related syndromes. Each of the analyzed probands had at least another family member with PDB, showing vertical transmission, which is consistent with the autosomal-dominant inheritance pattern of the disease. Mutation analysis identified the c.2810C>G mutation in one proband (II-1, family 2) ([Figure 1A](#)) and a new mutation, c.725G>T (p.Ser242Ile), in exon 2 of *ZNF687* in a different proband (family 3) ([Figure 2A](#)). The c.2810C>G mutation segregated with the disease phenotype in family 2; it was detected in the affected relative (II-3) but not in his healthy brother (II-2). The proband (II-6) and all affected siblings (II-1 and II-3) of family 3 were heterozygous for the *ZNF687* c.725G>T missense mutation. This mutation was not detected in the three unaffected family members (II-2, II-4, and II-5) of family 3 ([Figures 2A](#) and [2B](#)) and was not reported in the 1000 Genome and ExAC databases. The serine at the 242 position of *ZNF687* is highly conserved in all species ([Figure 2C](#)), and the p.Ser242Ile change was predicted in silico (by SIFT, PolyPhen, PMut, and Align GVGD) to be highly pathogenic, suggesting a causative role. Computational analysis strongly suggested Ser242 to be an important phosphorylation site (score of 0.996 in NetPhos prediction).²⁰ Subsequently, both the c.2810C>G and c.725G>T mutations were screened by TaqMan assay in two cohorts of PDB-affected individuals of different ethnicity. The c.2810C>G mutation was found in two out of 615 Italian individuals with PDB and two out of 339 individuals from a multiethnic North-American PDB-affected cohort. Both mutations were absent in chromosome samples from the two cohorts of control individuals of Italian and North-American origin. All these data suggest that *ZNF687* mutations are present in a subset of individuals with familial PDB and more rarely in individuals with sporadic PDB. Moreover, most individuals with *ZNF687* mutations showed a severe form of PDB, with an earlier onset and greater number of affected skeletal sites than individuals with or without *SQSTM1* mutations ([Table 1](#) and [Figure 2D](#)).

Role of *ZNF687* in Bone Metabolism

The expression profile of *ZNF687* was evidenced by real-time PCR in all examined adult human tissues, including bone ([Figure S3](#)). To investigate *ZNF687* mRNA expression during osteoclast formation, PBMCs from healthy

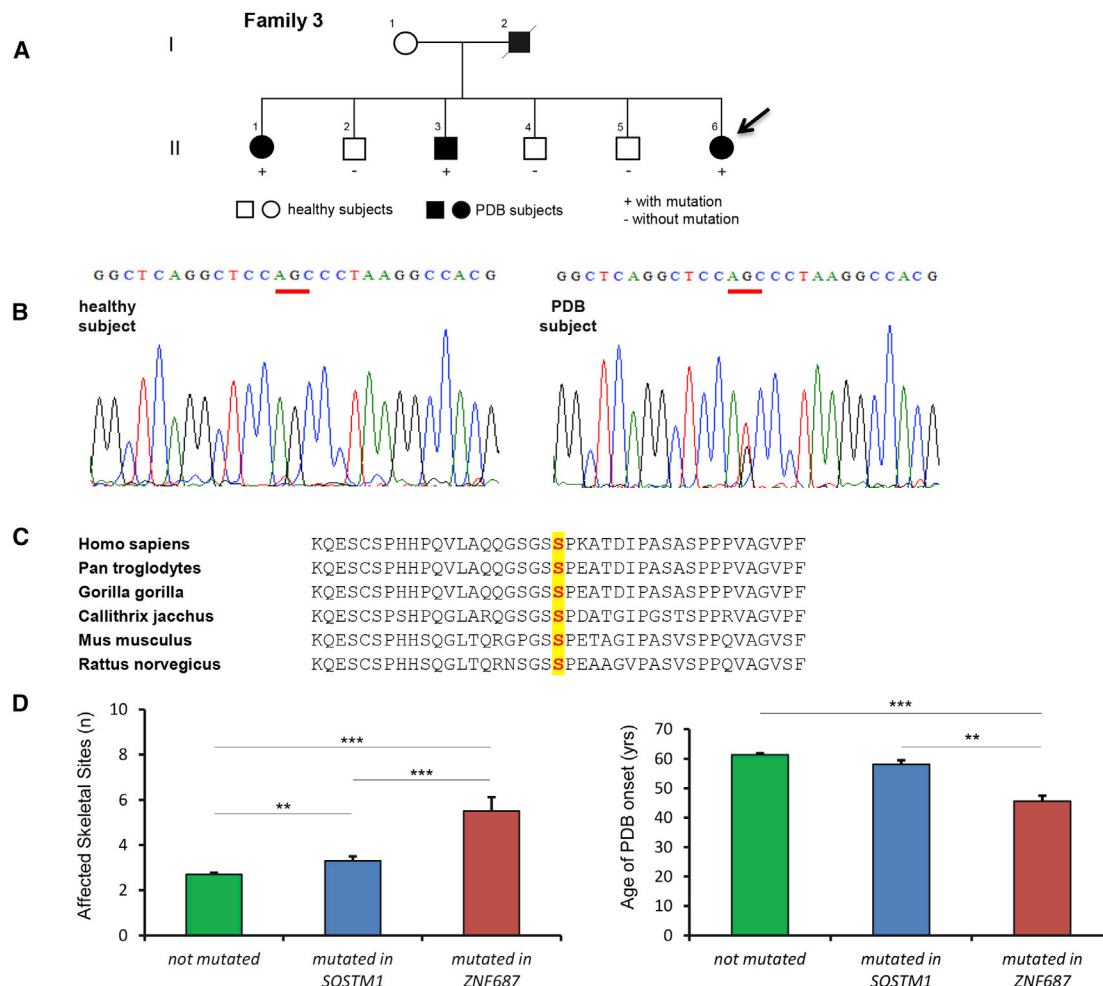


Figure 2. Identification of the c.725G>T Mutation in *ZNF687*

(A) The pedigree of family 3. The index individual is indicated by an arrow. Individuals with PDB are indicated by black symbols, and individuals without PDB are shown as unfilled symbols. Circles represent females, squares represent males, and slashes indicate deceased subjects.

(B) The DNA sequence of a segment flanking c.725G>T in *ZNF687* from an unaffected family member (left) and a heterozygous PDB-affected individual (right). A single base substitution changes the non-mutant guanine to thymine, leading to the substitution of serine (S) for isoleucine (I) at the 242 codon (indicated by a solid line).

(C) The evolutionary conservation of the 242 serine from rodents to humans.

(D) The number of the affected skeletal sites (left) and the age of disease onset (right) across PDB-affected individuals with *ZNF687* mutations, PDB-affected individuals with *SQSTM1* mutations, and PDB-affected individuals without mutations in either gene. Genotype-phenotype correlations were tested by ANOVA with Bonferroni correction and reported as mean ratio ± SEM (not mutated, n = 615; mutated in *SQSTM1*, n = 78; mutated in *ZNF687*, n = 20). *p < 0.05; **p < 0.01; ***p < 0.001.

volunteers were induced to osteoclastogenesis by treatment with M-CSF and sRANKL. Osteoclastogenesis was assessed by TRAP staining as described in [Subjects and Methods](#). Our results showed that, after treatment with M-CSF and RANKL, *ZNF687* expression was significantly increased ([Figure 3A](#)). Furthermore, given that GCT derives from the uncontrolled proliferation of mesenchymal stromal cells committed toward osteoblastic lineage, we also evaluated *ZNF687* expression during osteoblastogenesis. As expected, *ZNF687* mRNA expression was higher in differentiated osteoblasts than in their undifferentiated precursors ([Figure 3B](#)). Collectively, these data indicate that *ZNF687* plays a role in bone metabolism and that it is highly expressed during osteoclast and osteoblast differ-

entiation. To further verify this, we evaluated the expression levels of the two zebrafish orthologs (*ZNF687a* and *ZNF687b*) during *Danio rerio* development and during tissue regeneration (blastema), after caudal fin amputation. Both genes showed high expression levels during the regeneration of the caudal fin ([Figures 3C and 3D](#)), suggesting a possible role in cell proliferation and differentiation. Consistent with this observation, both genes appeared to be maternally inherited and highly expressed in the initial stages of zebrafish development. Interestingly, expression of *ZNF687a* increased again between 24 hr and 5 dpf and after 20 dpf, when hematopoiesis and osteoclastogenesis are known to occur in zebrafish ([Figure 3E](#)).²³ Accordingly, *ZNF687a* was also highly expressed in adult kidney and

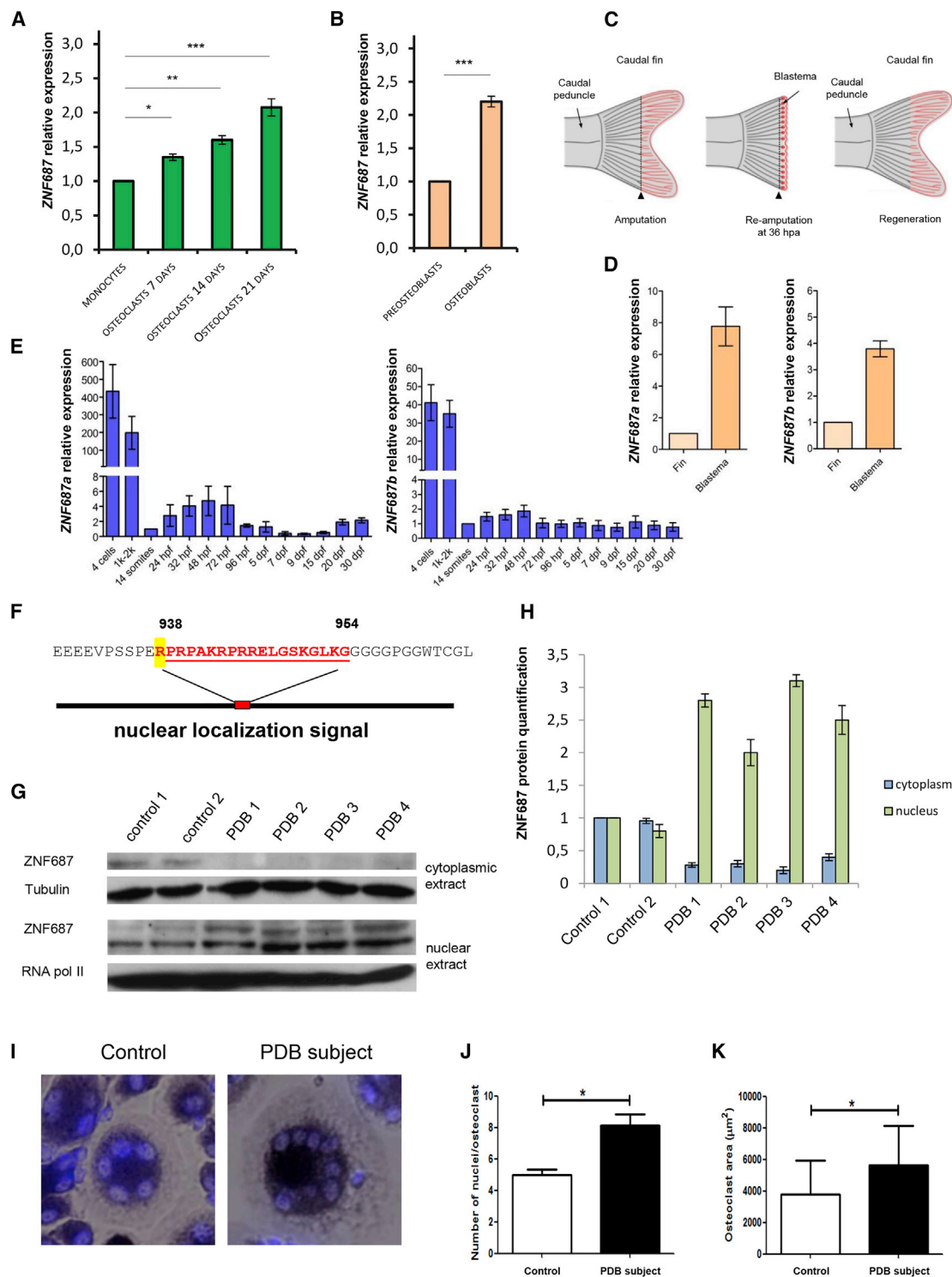


Figure 3. Expression and Functional Characterization of ZNF687

(A and B) Expression analysis of ZNF687 during human osteoclastogenesis (A) and human osteoblastogenesis (B). The data shown are representative of three independent experiments and were analyzed by Student's t test.

(C and D) The scheme of caudal fin regeneration in zebrafish (*Danio rerio*) (C) and the expression of ZNF687a and ZNF687b (zebrafish orthologs) during this process (D).

(E) ZNF687a and ZNF687b expression during *Danio rerio* development.

(F) Bioinformatic prediction of the NLS in ZNF687 between amino acids 938 and 955 enhanced as a consequence of the substitution of arginine at the 937 position.

(G) The expression of ZNF687 in nuclear- and cytoplasmic-extracts in lymphoblastic cell lines derived from affected individuals with the p.Pro937Arg change (PDB-affected individuals 1–4) in comparison to expression in those derived from healthy subjects (control individuals 1 and 2). ZNF687 antibody detected one band of about 135 kDa in the cytoplasm and two bands of about 100 and 135 kDa in the nucleus. Cytoplasm and nuclear extracts contained only minimal or no contamination (data not shown).

(legend continued on next page)

spleen tissues, the major organs for proliferation and differentiation of the hematopoietic cells, including osteoclast precursors (Figure S4).

Functional Consequences of *ZNF687* Mutation

Bioinformatic analysis suggested that *ZNF687* contains a strong nuclear localization signal (NLS) sequence between amino acids 938 and 954 (Figure 3F). The substitution of the arginine at the 937 position generates a stronger NLS that could enhance *ZNF687* nuclear import. Therefore, we performed cellular protein fractionation analysis followed by Western blotting by using anti-*ZNF687* antibody. Our analysis revealed *ZNF687* to be less prominent in the cytoplasmic fraction in lymphoblastic cell lines derived from PDB-affected individuals with c.2810C>G mutation than in those derived from control individuals (Figures 3G and 3H). We also found a parallel increase of *ZNF687* in the nuclear fraction, suggesting that c.2810C>G acts as gain-of-function mutation, altering the nuclear-cytoplasmic balance of *ZNF687*, thus leading to enhanced availability of this transcription factor in the nucleus. To directly test the causal link between the c.2810C>G mutation in *ZNF687* and the osteoclast differentiation process, human PBMCs, derived from five PDB-affected individuals carrying the c.2810C>G mutation, were differentiated into osteoclasts in the presence of sRANKL and M-CSF cytokines. Interestingly, osteoclasts cultured from these individuals showed a greater number of nuclei (Figures 3I–3J) as well as a larger surface area (Figures 3I and 3K) than did those from the control individuals, both features being peculiar for pagetic osteoclasts.

Increased *ZNF687* Expression in PDB-Affected Individuals

Given that PDB is a disease of the osteoclast and *ZNF687* is upregulated during osteoclastogenesis, we evaluated *ZNF687* expression in PDB-affected individuals with different genetic backgrounds. Using real-time PCR, we assessed the expression level of *ZNF687* in PBMCs from six PDB-affected individuals without a *SQSTM1* mutation, five PDB-affected individuals with a *SQSTM1* mutation, five PDB-affected individuals with a *ZNF687* mutation, and three healthy subjects. Of interest, *ZNF687* expression levels were significantly higher in PDB-affected individuals with (3-fold) or without (2-fold) an *SQSTM1* mutation than in the control individuals (Figure 4A and Figure S5). Moreover, a larger increase (5-fold) was observed in PDB-affected individuals exhibiting the c.2810C>G mutation in *ZNF687* (Figure 4A and Figure S5). These results suggest that *ZNF687* is involved in PDB pathogenesis regardless of the genetic background of PDB-affected individuals. Its expression profile remarkably correlates with the clinical

severity of the disease. To further clarify *ZNF687* involvement in PDB pathogenesis, we first analyzed the ChIPBase database, an integrated platform for decoding transcription factor binding sites (including 11 independent ChIP-seq experiments of NFκB transcription factor).²⁴ Interestingly, in all experiments, *ZNF687* was detected as a genomic target of NFκB in its putative promoter (Figure 4B). Similar to *ZNF687*, *ZMYND8* (MIM: 615713) and *ZNF592* (MIM: 613624), the other two partners of *ZNF687* in the Z3 complex formation, are regulated by NFκB transcription factor, which binds their promoters (data not shown). Next, we evaluated *ZNF687* expression in tumor tissues derived from five individuals with GCT/PDB. As expected, in comparison to expression in healthy bone marrow, a dramatic increase in *ZNF687* expression was observed in the RNAs extracted from tumor biopsies of these individuals, confirming the pathological role of *ZNF687*, whose expression resulted from the c.2810C>G mutation (Figure 4C). These data were reinforced by immunohistochemistry assays performed on tumor sections of the same GCT/PDB-affected individuals, in which we observed stronger *ZNF687* staining in the pathological giant cells than in the stromal cells, in comparison to the negative section (Figures 4D and 4E).

Discussion

Neoplastic transformation is a rare but serious complication of PDB, occurring in less than 1% of PDB-affected individuals. In a recent analysis of the cumulative survival curves of GCT occurring in individuals with or without PDB, we demonstrated that about half of PDB-affected individuals die within five years of the diagnosis of GCT, increasing to 80% after ten years.⁷ Here, we identify a pathogenic missense mutation in *ZNF687* (c.2810C>G) in a large pagetic family characterized by an enhanced prevalence of GCT in up to 30% of affected members. The same mutation was also identified in all the tested unrelated individuals with PDB and GCT, as well as in one individual with PDB and a positive family history of GCT. Moreover, replication analysis identified the *ZNF687* c.2810C>G mutation and a new *ZNF687* mutation (c.725G>T) in two families with a clear family history for PDB. A further analysis of two large cohorts of unrelated PDB-affected individuals with different ethnic backgrounds identified the *ZNF687* c.2810C>G mutation in 0.3% and 0.6% of cases, respectively. All individuals harboring mutations, except one, had polyostotic disorder with a significantly increased number of affected skeletal sites and an earlier onset of disease than PDB-affected individuals without the mutation, including PDB-affected individuals with the *SQSTM1* mutation. Taken together,

(H) The quantifications of cytoplasmic and nuclear fractions.

(I–K) The increased number of nuclei and the increased cellular area of osteoclasts derived from PDB subjects carrying the c.2810C>G mutation compared to the controls.

p* < 0.05; *p* < 0.01; ****p* < 0.001.

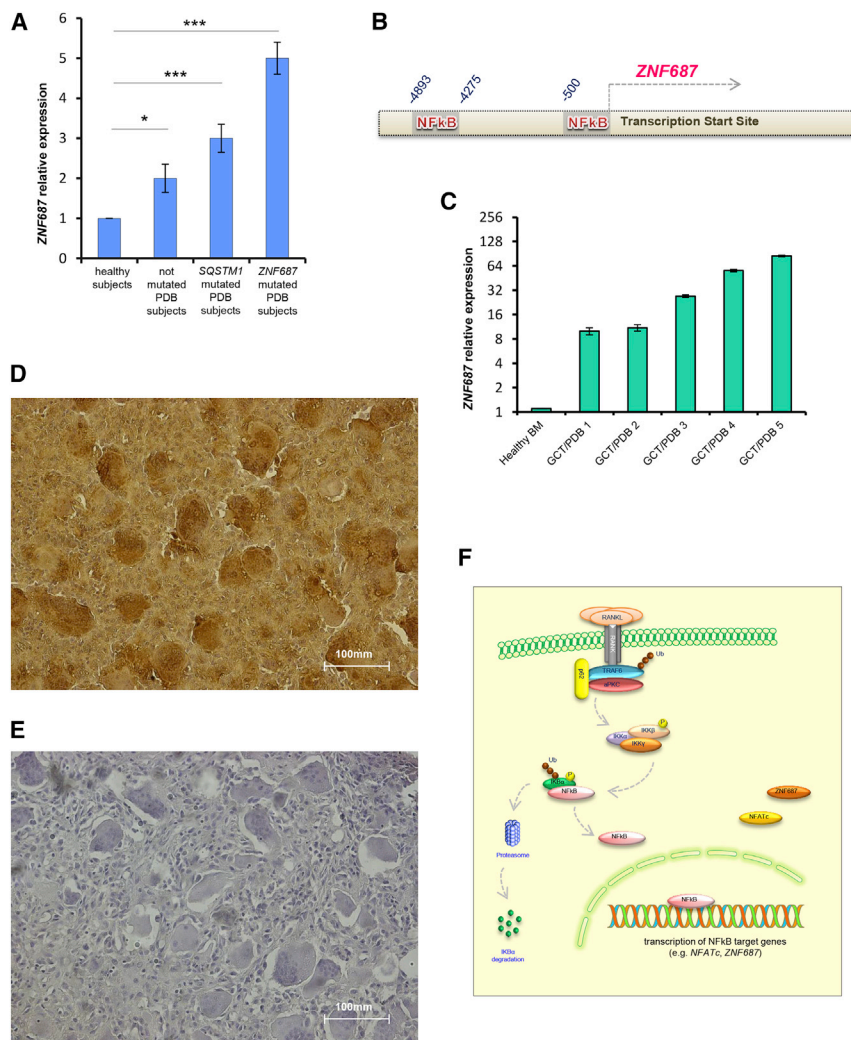


Figure 4. Upregulation of ZNF687 in Peripheral Blood of PDB-Affected Subjects and in Tumor Tissues of GCT/PDB-Affected Individuals

(A) The expression of ZNF687 in peripheral blood from healthy subjects, PDB-affected individuals without SQSTM1 or ZNF687 mutations, PDB-affected individuals with an SQSTM1 mutation, and PDB-affected individuals with a ZNF687 mutation. * = $p < 0.05$; ** = $p < 0.01$; *** = $p < 0.001$.

(B) NFκB binding sites on the ZNF687 promoter region.

(C) The expression profile of ZNF687 in frozen tumor tissues from five GCT/PDB-affected individuals in comparison to the expression in tissue from healthy bone marrow.

(D and E) ZNF687 expression on a tumor biopsy of a GCT/PDB-affected individual (D) in comparison to the tumor section derived from the same individual without primary antibody (negative control).

(F) A hypothetical model of ZNF687 involvement in the PDB molecular pathway.

these results indicate that mutations in ZNF687 are associated with severe PDB, with a prevalence of 3/31 (10%) in our familial cases with a documented autosomal-dominant pattern of inheritance, whereas they occur rarely in non-familial disease. Given that all the individuals with PDB and GCT tested in this study were positive for the mutation, we conclude that this ZNF687 mutation is responsible for severe PDB, sometimes complicated by GCT, in the presence of an impaired response to antiresorptive treatment.¹²

ZNF687 encodes a C2H2 zinc finger protein expressed in most tissues, including bone, that, together with ZMYND8 and ZNF592, is part of the transcriptional regulator complex Z3.²¹ Despite different C2H2 zinc finger proteins being identified as important regulators of skeletal development and maintenance, the role of ZNF687 in bone metabolism has never been identified.²⁵ Our in vitro and in vivo findings indicate that ZNF687 has bone regulatory properties. First, it is upregulated during osteoclast and osteoblast differentiation and is highly expressed during the regeneration of caudal fins in zebrafish, suggesting a role of this transcriptional co-regulator in bone cell prolif-

eration and differentiation. Moreover, ZNF687 has been shown to be overexpressed in all the tested PBMC samples derived from PDB-affected individuals, irrespective of the genetic defect, given that this gene is a downstream target of NFκB, allowing us to hypothesize the mechanism reported in Figure 4F.

The exact mechanism by which ZNF687 mutations cause PDB and eventually GCT remains unknown.

Because a stronger NLS was observed in the presence of the proline to arginine substitution at the 937 position, we hypothesize that the mutation acts as a gain of function, leading to the constitutive accumulation of ZNF687 in the nucleus, thus increasing the transcription of its downstream targets, which in turn might promote the development of the disorder. Remarkably, osteoclasts derived from PBMCs of PDB-affected individuals with the c.2810C>G mutation in ZNF687 were increased in size and contained more nuclei than normal osteoclasts, which are both features of osteoclasts isolated from pagetic tissue.^{1–3} These data suggest that the c.2810C>G mutation might contribute to PDB susceptibility by affecting osteoclast phenotype.

In addition, considering that we identified the c.725G>T mutation in familial individuals only affected by PDB, we hypothesized that c.725G>T mutation is responsible for the onset of PDB, but not associated with GCT development. Therefore, we speculated that, differently from the c.2810C>G mutation, the biological defect of c.725G>T does not result in the neoplastic transformation of PDB tissue. Further functional studies are required

to address this point as well as the biological difference with the c.2810C>G mutation.

In conclusion, in this study we identified mutations in *ZNF687* as a monogenic cause of a severe, early-onset form of PDB, which is associated in some instances (c.2810C>G mutation) with an increased likelihood of GCT. This evidence, together with our in vitro and in vivo experimental observations, emphasizes a previously unexpected role of *ZNF687* in bone metabolism. It would be of interest to determine the *ZNF687* role in other neoplastic conditions related to PDB, such as osteosarcoma, that, like GCT, are due to the malignant transformation of mesenchymal stromal cells.

Finally, a better characterization of the downstream pathways regulated by this transcriptional co-regulator in bone cells might be relevant for the identification of new therapeutic targets for PDB and other disorders of skeletal metabolism.

Supplemental Data

Supplemental Data include five figures and five tables and can be found with this article online at <http://dx.doi.org/10.1016/j.ajhg.2015.12.016>.

Acknowledgments

We thank Dr. Monica Autiero for helpful suggestions and manuscript editing, Mrs. Edith Gagnon at Québec Research Centre for Sanger sequencing, Dr. Riccardo Muscariello at the Department of Medicine and Surgery at Federico II University for recruitment of PDB-affected individuals, and Dr. Federica Scotto di Carlo for her assistance in submitting this paper. This work was supported by Telethon Italy (grant no. 11119A, F.G. and L.G.), the European Calcified Tissue Society/AMGEN fellowship (F.G.), the Italian Society for Osteoporosis, Mineral Metabolism and Skeletal Diseases (F.G.), the John G. Haddad Research Award from the Paget Foundation (L.G.), and the Italian Association for Cancer Research (grant IG-2014 no.15707, F.G.). The Short-term Mobility Program from the Italian National Research Council (F.G.) is gratefully acknowledged, as well as the Galliera Genetic Bank funded by Telethon Italy (grant no. GTB12001). This work is dedicated to the memory of Dr. Giuseppe Mossetti.

Received: September 15, 2015

Accepted: December 17, 2015

Published: February 4, 2016

Web Resources

The URLs for data presented herein are as follows:

1000 Genomes, <http://browser.1000genomes.org>

ChIPBase database, <http://deepbase.sysu.edu.cn/chipbase/index.php>

ExAC Browser, <http://exac.broadinstitute.org/>

GenBank, <http://www.ncbi.nlm.nih.gov/genbank/>

NetPhos 2.0, <http://www.cbs.dtu.dk/services/NetPhos/>

NLStradamus, <http://www.moseslab.csb.utoronto.ca/NLStradamus/>

OMIM, <http://www.omim.org/>

UCSC Genome Browser, <http://genome.ucsc.edu>

References

1. Ralston, S.H. (2013). Clinical practice. Paget's disease of bone. *N. Engl. J. Med.* 368, 644–650.
2. Roodman, G.D., and Windle, J.J. (2005). Paget disease of bone. *J. Clin. Invest.* 115, 200–208.
3. Whyte, M.P. (2006). Clinical practice. Paget's disease of bone. *N. Engl. J. Med.* 355, 593–600.
4. Hansen, M.F., Seton, M., and Merchant, A. (2006). Osteosarcoma in Paget's disease of bone. *J. Bone Miner. Res.* 21 (Suppl 2), 58–63.
5. Jacobs, T.P., Michelsen, J., Polay, J.S., D'Adamo, A.C., and Canfield, R.E. (1979). Giant cell tumor in Paget's disease of bone: familial and geographic clustering. *Cancer* 44, 742–747.
6. Gebhart, M., Vandeweyer, E., and Nemec, E. (1998). Paget's disease of bone complicated by giant cell tumor. *Clin. Orthop. Relat. Res.* (352), 187–193.
7. Rendina, D., De Filippo, G., Ralston, S.H., Merlotti, D., Gianfrancesco, F., Esposito, T., Muscariello, R., Nuti, R., Strazzullo, P., and Gennari, L. (2015). Clinical characteristics and evolution of giant cell tumor occurring in Paget's disease of bone. *J. Bone Miner. Res.* 30, 257–263.
8. Laurin, N., Brown, J.P., Morissette, J., and Raymond, V. (2002). Recurrent mutation of the gene encoding sequestosome 1 (SQSTM1/p62) in Paget disease of bone. *Am. J. Hum. Genet.* 70, 1582–1588.
9. Hocking, L.J., Lucas, G.J., Daroszewska, A., Mangion, J., Olavsen, M., Cundy, T., Nicholson, G.C., Ward, L., Bennett, S.T., Wuyts, W., et al. (2002). Domain-specific mutations in sequestosome 1 (SQSTM1) cause familial and sporadic Paget's disease. *Hum. Mol. Genet.* 11, 2735–2739.
10. Albagha, O.M., Visconti, M.R., Alonso, N., Langston, A.L., Cundy, T., Dargie, R., Dunlop, M.G., Fraser, W.D., Hooper, M.J., Isaia, G., et al. (2010). Genome-wide association study identifies variants at CSF1, OPTN and TNFRSF11A as genetic risk factors for Paget's disease of bone. *Nat. Genet.* 42, 520–524.
11. Albagha, O.M., Wani, S.E., Visconti, M.R., Alonso, N., Goodman, K., Brandi, M.L., Cundy, T., Chung, P.Y., Dargie, R., Devogelaer, J.P., et al.; Genetic Determinants of Paget's Disease (GDPD) Consortium (2011). Genome-wide association identifies three new susceptibility loci for Paget's disease of bone. *Nat. Genet.* 43, 685–689.
12. Gianfrancesco, F., Rendina, D., Merlotti, D., Esposito, T., Amyere, M., Formicola, D., Muscariello, R., De Filippo, G., Strazzullo, P., Nuti, R., et al. (2013). Giant cell tumor occurring in familial Paget's disease of bone: report of clinical characteristics and linkage analysis of a large pedigree. *J. Bone Miner. Res.* 28, 341–350.
13. Whyte, M.P. (2006). Paget's disease of bone and genetic disorders of RANKL/OPG/RANK/NF-kappaB signaling. *Ann. N Y Acad. Sci.* 1068, 143–164.
14. Gennari, L., Gianfrancesco, F., Di Stefano, M., Rendina, D., Merlotti, D., Esposito, T., Gallone, S., Fusco, P., Rainero, I., Fenoglio, P., et al. (2010). SQSTM1 gene analysis and gene-environment interaction in Paget's disease of bone. *J. Bone Miner. Res.* 25, 1375–1384.
15. Michou, L., Morissette, J., Gagnon, E.R., Marquis, A., Dellabada, M., Brown, J.P., and Siris, E.S. (2011). Novel SQSTM1 mutations in patients with Paget's disease of bone in an unrelated multiethnic American population. *Bone* 48, 456–460.
16. Esposito, T., Lea, R.A., Maher, B.H., Moses, D., Cox, H.C., Magliocca, S., Angius, A., Nyholt, D.R., Titus, T., Kay, T., et al.

- (2013). Unique X-linked familial FSGS with co-segregating heart block disorder is associated with a mutation in the NXF5 gene. *Hum. Mol. Genet.* **22**, 3654–3666.
17. Esposito, T., Sampaolo, S., Limongelli, G., Varone, A., Formicola, D., Diodato, D., Farina, O., Napolitano, F., Pacileo, G., Gianfrancesco, F., and Di Iorio, G. (2013). Digenic mutational inheritance of the integrin alpha 7 and the myosin heavy chain 7B genes causes congenital myopathy with left ventricular non-compact cardiomyopathy. *Orphanet J. Rare Dis.* **8**, 91.
 18. Nguyen Ba, A.N., Pogoutse, A., Provar, N., and Moses, A.M. (2009). NLStradamus: a simple Hidden Markov Model for nuclear localization signal prediction. *BMC Bioinformatics* **10**, 202.
 19. Kirby, T.W., Gassman, N.R., Smith, C.E., Pedersen, L.C., Gabel, S.A., Sobhany, M., Wilson, S.H., and London, R.E. (2015). Nuclear Localization of the DNA Repair Scaffold XRCC1: Uncovering the Functional Role of a Bipartite NLS. *Sci. Rep.* **5**, 13405.
 20. Blom, N., Gammeltoft, S., and Brunak, S. (1999). Sequence and structure-based prediction of eukaryotic protein phosphorylation sites. *J. Mol. Biol.* **294**, 1351–1362.
 21. Malovannaya, A., Lanz, R.B., Jung, S.Y., Bulynko, Y., Le, N.T., Chan, D.W., Ding, C., Shi, Y., Yucer, N., Krenciute, G., et al. (2011). Analysis of the human endogenous coregulator complexome. *Cell* **145**, 787–799.
 22. Rendina, D., Gennari, L., De Filippo, G., Merlotti, D., de Campora, E., Fazioli, F., Scarano, G., Nuti, R., Strazzullo, P., and Mossetti, G. (2006). Evidence for increased clinical severity of familial and sporadic Paget's disease of bone in Campania, southern Italy. *J. Bone Miner. Res.* **21**, 1828–1835.
 23. Bertrand, J.Y., Kim, A.D., Violette, E.P., Stachura, D.L., Cisson, J.L., and Traver, D. (2007). Definitive hematopoiesis initiates through a committed erythromyeloid progenitor in the zebrafish embryo. *Development* **134**, 4147–4156.
 24. Yang, J.H., Li, J.H., Jiang, S., Zhou, H., and Qu, L.H. (2013). ChIPBase: a database for decoding the transcriptional regulation of long non-coding RNA and microRNA genes from ChIP-Seq data. *Nucleic Acids Res.* **41**, D177–D187.
 25. Ganss, B., and Jheon, A. (2004). Zinc finger transcription factors in skeletal development. *Crit. Rev. Oral Biol. Med.* **15**, 282–297.